An Information Theoretical Analysis of Multi-terminal Neuro-spike Communication Network in Spinal Cord

Meltem Civas
Next-generation and Wireless Communications Laboratory (NWCL)
Department of Electrical and Electronics Engineering
Koç University
Istanbul, Turkey
mcivas16@ku.edu.tr

Ozgur B. Akan*
Internet of Everything (IoE) Group
Department of Engineering
University of Cambridge
Cambridge, UK
oba21@cam.ac.uk

ABSTRACT

Communication theoretical understanding of healthy and diseased connections in the spinal cord motor system is crucial for realizing future information and communication technology (ICT) based diagnosis and treatment techniques for spinal cord injuries (SCI). A spinal cord motor nucleus associated with a particular muscle constitutes an ideal candidate for studying to have an understanding of SCI. Typical spinal cord motor nucleus system contains pool of lower motor neurons (MNs) controlling a muscle by integrating synaptic inputs from spinal interneurons (INs), upper motor neurons (DNs) and sensory neurons (SNs). In this study, we consider this system from ICT perspective. Our aim is to quantify the rate of information flow across a spinal cord motor nucleus. To this end, we model an equivalent single-hop multiterminal network, where multiple transmitting nodes representing heterogeneous population of DNs, INs and SNs send information to multiple receiving nodes corresponding to MNs. To identify the outputs at receiving nodes, we define corresponding neurospike communication channel and then find the bound on total rates across this network. Based on the network model, we analyze achievable rates for a particular motor nucleus system called Tibialis Anterior (TA) motor nucleus in the spinal cord numerically and simulate several spinal cord dysfunction scenarios. The numerical results reveal that decrease in the maximum total rates with the lower motor neuron injury causes weakness in the affected muscle.

CCS CONCEPTS

• **Computing methodologies** → **Modeling and simulation**;

KEYWORDS

Spinal Cord Injuries, ICT-based treatments, Nanonetworks, Multi-terminal networks, Neuro-spike communication

*Also with , Next-generation and Wireless Communications Laboratory (NWCL), Department of Electrical and Electronics Engineering, Koç University.

NANOCOM '18, September 5–7, 2018, Reykjavik, Iceland

ACM ISBN 978-1-4503-5711-1/18/09…$15.00
https://doi.org/10.1145/3233188.3233215

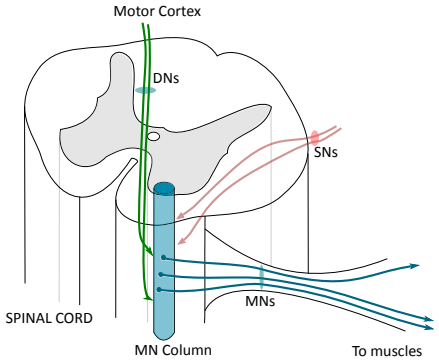

Figure 1: Spinal cord motor nucleus system

ACM Reference Format:
Meltem Civas and Ozgur B. Akan. 2018. An Information Theoretical Analysis of Multi-terminal Neuro-spike Communication Network in Spinal Cord. In *NANOCOM '18: NANOCOM '18: ACM The Fifth Annual International Conference on Nanoscale Computing and Communication, September 5–7, 2018, Reykjavik, Iceland*. ACM, New York, NY, USA, 6 pages. https://doi.org/10.1145/3233188.3233215

1 INTRODUCTION

Advancements in nanotechnology have enabled the deployment of nanonetworks comprising of nanomachines with biologically inspired capabilities inside human body. In this respect, Internet of Bio-Nano Things (IoBNT) framework was proposed [2, 3] as the basis for future applications including ICT-based diagnosis tools and treatment techniques for SCI. Deployment of replacement-nanomachines as an ICT-based solution to SCI requires understanding of healthy and interrupted neural connections from ICT perspective. To this end, extensive research effort has focused on the modeling and analysis of neuro-spike communication [6, 17, 19, 28–31] and other physical and conceptual communication models for neural communication [1, 7, 9, 35, 37].

Specifically, brain and neurons of spinal cord have been modeled as cloud and fog nodes based on the analogy between cloud and fog networking architecture in [7]. In [35], to recover communication failures through spinal cord sensory pathways, replacement neural network using time division multiple access has been proposed. However, a realistic communication network model for spinal cord system taking physiological characteristics of neurons into account is not considered in the literature to our knowledge.

Spinal cord system comprises of complex networks including motor circuits, which involve in execution of motor actions such as locomotion and postural control by integrating inputs from periphery neurons and brain. Spinal motoneurons, MNs, are the final common pathway where whole information is resolved. Spinal cord motor system consists of several motor nuclei each of which having group of MNs controlling a particular muscle group [10]. When the communication fails through a particular motor nucleus, its effects can be monitored directly on the corresponding muscle. Main synaptic inputs to a typical motor nucleus system are conveyed from the periphery via SNs, from the brain via DNs as illustrated in Fig. 1. Moreover, INs relay inputs from the spinal cord to MNs.

In this paper, our aim is to quantify the bound on the information flow across a spinal cord motor nucleus system. To this aim, we model equivalent neuro-spike communication network to a motor nucleus system as a single-hop multi terminal network consisting of multiple transmitting and receiving nodes corresponding to presynaptic and postsynaptic neurons, respectively. The inputs to the equivalent channel are spike trains transmitted by the transmitting nodes and the outputs are spike trains generated at the receiving nodes. Utilizing the neuro-spike communication model describing vesicle release from presynaptic neuron, post-synaptic filtering and postsynaptic spike generation, we find the output at each receiving node. Using this, we derive a bound on the total achievable rate across the network. Based on the neuron quantities in the spinal cord TA motor nucleus as shown in Table 1 and realistic biophysical channel parameters for each class of neurons in the system, we analyze effects of different class of presynaptic and postsynaptic neurons on the total maximum achievable rates.

The main motivation behind this study is finding relationship between the information theoretical metrics and several spinal cord dysfunctions. Hence, we simulate several spinal cord diseases by changing the number of receiving and transmitting nodes. Then, we find relations between information theoretical metrics and spinal cord dysfunctions. The results reveal that when part of MNs is injured, decreasing total maximum rate results in weakness in the muscle. These results may help in designing ICT-based diagnosis and treatment techniques. To our knowledge, this is the first work studying a spinal cord system from neuro-spike communication perspective.

The rest of the paper is organized as follows. Section 2 describes the equivalent network model for spinal cord motor nucleus. In Section 3, bound on the total rate across the network is formulated. In Section 4, numerical results are discussed. Finally, conclusions are stated in Section 5.

2 NEURO-SPIKE COMMUNICATION NETWORK MODEL OF THE MOTOR NUCLEUS SYSTEM

We consider a single-hop multi-terminal neuro-spike communication network where M transmitting nodes want to send information to K receiving nodes. Thus, transmitting nodes only transmit, whereas receiving nodes only receive. Transmitting nodes represent heterogeneous population of presynaptic SNs, INs, DNs. Receiving nodes correspond to postsynaptic MNs.

Table 1: Types of Excitatory (Ex) and Inhibitory (Inh) Neurons (TA motor nucleus) [10]

Class of Neuron	Ex/Inh	Quantity
SN (Ia afferent)	Ex	280
IN (Ib interneuron)	Inh	350
IN (Ia interneuron)	Inh	350
MN (S, FF, FR)	-	350

Transmitted input spike train to the channel, S_i, is associated with transmitting node i, where $i \in \mathcal{M} = \{1, 2, .., M\}$. We assume that inputs to the channel are independent. The spike train output of the channel Y_j is associated with receiving node j, where $j \in \mathcal{K} = \{1, 2, .., K\}$. Transmitting node i sends information to receiving node j at rate R_{ij}. The channel is memoryless with the channel transition function $P(Y^{\mathcal{K}}|S^{\mathcal{M}}) = P(Y_1, Y_2, ..., Y_K|S_1, S_2, ..., S_M)$. The channel considered is illustrated in Fig. 2. Possible links in the network are {SN→MN, IN→MN, DN→MN}. Each class of link is under a connectivity probability. $p_{\text{SM}}, p_{\text{IM}}$ and p_{DM} denote connectivity probabilities for {SN→MN, IN→MN, DN→MN}, respectively. The connectivity matrix, $\mathbf{X} = [X_{i,j}]$ contains connectivity state of each class of links. Accordingly, $X_{i,j}$ takes value of 1 if the synaptic connection exists and takes 0 otherwise for each $i \in \mathcal{M}$ and $j \in \mathcal{K}$.

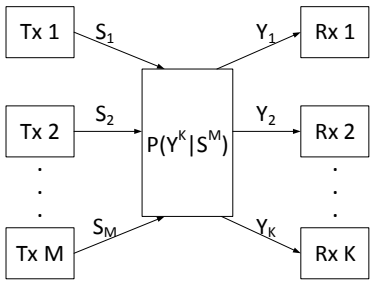

Figure 2: Considered one-hop multi-terminal network consisting of transmitting (left) and receiving nodes (right)

In order to derive the outputs accessed by the receiving nodes, we first need to define inputs to the channel given in Fig. 2 and then describe the channel model. Inputs and outputs of the channel are utilized in finding the bound on the total rate of information flow across the network. For point-to-point links in the network, we use existing neuro-spike channel blocks in the literature [6, 17, 19, 28–31] that are applicable to the spinal cord synapses.

Neuro-spike communication channels comprise of cascade stages, namely, axonal transmission, vesicle release, postsynaptic filtering and spike generation at the post-synaptic neuron. Presynaptic terminal refers to the part of presynaptic neuron where vesicles are released. Vesicles contain chemical substances called neurotransmitters, which diffuse through a specialized gap called synaptic cleft. Reaching postsynaptic terminal, neurotransmitters bind to the receptors located there, which generate potential at the postsynaptic membrane. When the membrane potential reaches the threshold value, the output spike is generated at the postsynaptic neuron. In

the following parts, we describe the neuro-spike channel model under consideration and derive the outputs at receiving nodes.

2.1 Presynaptic Inputs

Transmitting node or presynaptic neuron i generates Poisson spike train, $S_i(t)$, with rate λ_i, where $i \in \mathcal{M}$. For each neuron, λ_i is constrained such that $0 \leq \lambda_i \leq \lambda_{\max,i}$, where $\lambda_{\max,i}$ is maximum firing rate of the presynaptic neuron i. The limitation on the firing rate arises from *refractory period*, which is the minimum time period between any successive spikes [27]. Thus, time window can be divided into small windows with the length of Δt such that at most one spike can occur in Δt [30]. Therefore, probability of a spike in the nth time window is $P\{S_i[n] = 1\} = 1 - \exp(\lambda_i \Delta t)$. Spike train then propagates to presynaptic terminal, where vesicle release takes place, through the axon. Axonal transmission is considered reliable [36].

2.2 Vesicle Release

Probability of vesicle release from a release site is governed by available vesicles for release in the pool-based model [20]. Since dynamic synapses are not in the scope of this paper, we assume that size of readily releasable pool at a release site is constant. We adopt the term *functional contact* to refer any vesicle release sites associated with a presynaptic neuron as used in the [38]. From each functional contact of a typical IN, SN and DN, at most one vesicle is released when a spike arrives to a presynaptic terminal [4, 32]. Moreover, typical IN, SN and DN can make multiple functional contacts with postsynaptic MN [24, 32].

Considering the transmission from transmitting node i to receiving node j, the probability of a vesicle release at a single functional contact upon the arrival of a spike during nth time window is $P_{\text{rel},i} \triangleq P\{V_{i,j}[n] = 1 | S_i[n] = 1\}$. In case of multiple independent functional contacts, probability of k vesicle releases from T_i functional contacts follows Poisson binomial distribution [28, 31] as described by the following equation.

$$P\{V_{i,j}[n] = k | S_i[n] = 1\} = \frac{1}{T_i + 1} \sum_{l=0}^{T_i} F^{-lk} \prod_{m=1}^{T_i} (1 + (F^l - 1) P_{i,m}), \tag{1}$$

where $F = \exp(\frac{2\sqrt{-1}\pi}{T_i+1})$ and $P_{i,m}$ is the probability of release from mth functional contact of ith presynaptic neuron.

2.3 Postsynaptic Filtering

Neurotransmitter binding to postsynaptic receptors increases or decreases the membrane potential depending on the type of synapses. Thus, excitatory postsynaptic potential (EPSP) and inhibitory postsynaptic potential (IPSP) are generated at the postsynaptic neuron in excitatory and inhibitory synapses, respectively. Inhibitory and excitatory types of presynaptic neurons are shown in Table 1. Moreover, in {DN→MN} links, excitatory synapses occur.

Postsynaptic potential filtering at receiving node or postsynaptic neuron j due to access from transmitting node i is described by alpha function [19] as follows.

$$e_j(t) = w_{i,j} h_p \frac{t}{t_p} \exp(1 - \frac{t}{t_p}), t \geq 0 \tag{2}$$

where h_p and t_p are peak quantal amplitude and time to rise peak, respectively. $w_{i,j}$ is the weighting variable representing synaptic strength between transmitting node i and receiving node j. Values of quantal amplitude and rising time depend on the type of synapse. Thus, for the excitatory synapses, we define $h_p = h_{\text{ex}}$ and $t_p = t_{\text{ex}}$, whereas for the inhibitory synapses $h_p = h_{\text{inh}}$ and $t_p = t_{\text{inh}}$.

Synaptic strengths are characterized by morphology of synapses such as distribution of number of synapses and presynaptic terminal sizes [8]. Combined effect manifests itself as *lognormality*, which is reported for spinal cord motor circuits [23]. Thus, w, follows lognormal distribution with probability density function

$$f(w|\mu, \sigma) = \frac{1}{w\sigma\sqrt{2\pi}} \exp\left(\frac{-(\log w - \mu)^2}{2\sigma^2}\right); w > 0 \tag{3}$$

where $\mu = \log(\frac{m^2}{\sqrt{v+m^2}})$ is log mean and $\sigma = \sqrt{\log(\frac{v}{m^2+1})}$ is log variance, given m and v are mean and variance, respectively. w_{SM}, w_{IM} and w_{DM} are the lognormal random variables with corresponding mean and variance pairs $(m_{\text{SM}}, v_{\text{SM}}), (m_{\text{IM}}, v_{\text{IM}}), (m_{\text{DM}}, v_{\text{DM}})$ defined for each link in the set of synaptic links {SN→MN, IN→MN, DN→MN}, respectively.

2.4 Spike Generation

Membrane potential, $E_j(t)$, at receiving node j is spatiotemporal summation of contributions from each synaptic access in terms of EPSP and IPSP. Membrane potential is given by

$$\begin{aligned} E_j(t) = \theta_0 &+ \sum_{l \in \{\text{SN}\}} \sum_{t_n \leq t} w_{\text{SM},l,j} X_{l,j} V_{l,j}[n] h_{p,\text{ex}}(t - t_n) \\ &+ \sum_{i \in \{\text{IN}\}} \sum_{t_n \leq t} w_{\text{IN},i,j} X_{i,j} V_{i,j}[n] h_{p,\text{inh}}(t - t_n) \\ &+ \sum_{m \in \{\text{DN}\}} \sum_{t_n \leq t} w_{\text{DN},m,j} X_{m,j} V_{m,j}[n] h_{p,\text{ex}}(t - t_n) + z_j(t), \end{aligned} \tag{4}$$

where t_n is the beginning of nth time window. {SN}, {IN} and {DN} are the sets of SNs, INs and DNs in $\mathcal{M}$, respectively. $h_{p,\text{ex}}(t) = h_{\text{ex}} \exp(1 - \frac{t}{t_{\text{ex}}})$ and $h_{p,\text{inh}}(t) = h_{\text{inh}} \exp(1 - \frac{t}{t_{\text{inh}}})$ are EPSP and IPSP filters, respectively. θ_0 is the resting membrane potential and $z_j(t)$ is white Gaussian synaptic noise with variance σ_z^2. When $E_j(t)$ reaches the spiking threshold, θ_j, the postsynaptic neuron fires a spike, i.e., $Y_j[n] = 1$.

3 BOUND ON THE ACHIEVABLE RATES

In this part, we derive the bound on total achievable rates across the network using the cut-set bound.

We are given a cut $(\mathcal{M}, \mathcal{K})$. That is, nodes are already partitioned into two disjoint sets, namely, the set of transmitting nodes $\mathcal{M}$ consisting of SN, IN and DN nodes and the set of receiving nodes $\mathcal{K}$ consisting of MN nodes. By the defined cut, the channel reduces to multiple input multiple output (MIMO) channel so that total

information flow from $\mathcal{M}$ to $\mathcal{K}$ is bounded by the rate MIMO channel can support [12]. Thus, cut-set bound on the information flow from K transmitting nodes to M receiving nodes is given by the following [11].

$$\sum_{i\in\mathcal{M}, j\in\mathcal{K}} R_{ij} \leq I(S^{\mathcal{M}}[n]; Y^{\mathcal{K}}[n]), \tag{5}$$

where $S^{\mathcal{M}}[n] = \{S_1[n], S_2[n], ..., S_M[n]\}$ is the set of input spike trains to the channel and $Y^{\mathcal{K}}[n] = \{Y_1[n], Y_2[n], ..., Y_K[n]\}$ is the set of output spike trains at the nth time interval. $\{R_{ij}\}$ are achievable rates from transmitting node i to receiving node j and the bound is maximized over joint input distribution $p(S^{\mathcal{M}}[n])$. On the other hand, we know that the input spike trains, $S_i[n]$, are independent and Poisson distributed with λ_i. Thus, the right hand side in (5) is maximized over λ_i's.

Considering the channel model and the number of neurons, simulation of network scenario is highly complex. Thus, we perform numerical analysis of the network in the next section based on the following assumptions:

- Same class of neurons have identical biophysical properties, i.e., identical spiking rate, probability of release and number of functional contacts.
- All functional contacts of a presynaptic neuron are identical, i.e., $P_{i,m} = P_{\text{rel},i}, \forall m \in [1, T_i]$. Thus, vesicle release process reduces to Binomial release $B(T_i, P_{rel,i})$.

Therefore, number of output spikes at the receiving nodes depends only on the number of transmitted spikes by transmitting nodes. By definition, mutual information is

$$I(S^{\mathcal{M}}[n]; Y^{\mathcal{K}}[n]) = H(Y^{\mathcal{K}}[n]) - H(Y^{\mathcal{K}}[n]|S^{\mathcal{M}}[n]), \tag{6}$$

As a result of aforementioned assumptions, the conditional entropy in (6) is derived as

$$H(Y^{\mathcal{K}}[n]|S^{\mathcal{M}}[n]) = H(\sum_{i=1}^{K} Y_i[n] = s_m | \sum_{l=1}^{M} S_l[n] = s_s) \tag{7}$$

where s_m is number of output spikes at receiving nodes and s_s corresponds to number of input spikes transmitted by transmitting nodes.

4 NUMERICAL ANALYSIS

In this section, we evaluate performance of the network numerically with respect to maximum total achievable rate and mutual information. Based on the numerical results obtained, we discuss the spinal cord dysfunctions and the information theoretical metrics.

Probability of release is generally low (less than 0.3) at central synapses [4], thus, we use $p_D = 0.3$ for probability of release from DN. Moreover, we adopt $p_{\text{DM}} = 0.9$ based on the evidences that MNs have common projections from the brain [16]. Remaining parameters are given in Table 2.

Throughout the simulations, unless otherwise stated, we assume that spiking activity occurs during a motor action, for which SNs and INs are spiking at mean rates of $\lambda_{\text{SN}} = 80$ Hz [25] and $\lambda_{\text{IN}} = 20$ Hz [26], respectively. Number of different class of neurons that are given in Table 1 are used in the simulations unless otherwise stated. Number of SNs, INs, DNs and MNs recruited in the network are denoted by $N_{\text{SN}}, N_{\text{IN}}, N_{\text{DN}}, N_{\text{MN}}$, respectively.

Table 2: Model and simulation parameters

Parameter	Symbol	Value
Spiking Threshold (MN)	θ	−46.02 mV [22]
Resting Potential (MN)	θ_0	−64.81 mV [22]
Noise standard deviation	σ_z	0.1 mV [19]
Discretization time step	Δt	4 ms [30]
Spike width	Δt_s	4 ms [30]
Functional contact (SN,IN)	T_S, T_I	8, 7 [15, 21]
Probability of release (IN)	p_I	0.5 [18]
Probability of release (SN)	p_S	0.5
Peak quantal EPSP	h_{ex}	0.1 mV [14]
Peak quantal IPSP	h_{inh}	−0.08 mV [18]
Time to peak of EPSP	t_{ex}	0.2 ms [15]
Time to peak of IPSP	t_{inh}	0.2 ms [34]
Connectivity: IN to MN	p_{IM}	0.2 [16]
Connectivity: SN to MN	p_{SM}	0.8 [13]
Mean of w (SN, IN, DN)	$m_{\text{SN}}, m_{\text{IN}}, m_{\text{DN}}$	1 [16]
Variance of w (SN, IN, DN)	$v_{\text{SN}}, v_{\text{IN}}, v_{\text{DN}}$	1 [16]

In the following part, we first analyze effects of number of lower motor neurons, MNs, on the maximum total achievable rate when the mutual information is simulated for different spiking rates of DNs, λ_{DN}. Secondly, we evaluate effects of number of DNs, upper motor neurons, and number of functional contacts per DN, T_D, on the maximum total achievable rate.

4.1 Maximum Total Rate versus Number of MNs

Fig. 3a shows mutual information versus λ_{DN} for different number of MNs. Around $\lambda_{\text{DN}} = 120$ Hz, mutual information is at the maximum. This value is comparable to the reported maximum spiking rate of DNs, that is $\lambda_{\text{DN,max}} \sim 106$ Hz (corticospinal pyramidal cells) [22]. Moreover, maximum total rate increases with the number of MNs, N_{MN}, as shown in Fig. 3b. With $N_{\text{MN}} = 350$, which is the quantity referring to the TA nucleus as given in Table 1, bound on the total rate is ~ 1.3 bits per network use.

General design considerations with regard to synaptic nanonetworks include that multiterminal network capacity can be increased with number of receiving nodes deployed in the network, considering the result depicted in Fig. 3b.

4.2 Maximum Total Rate versus Number of DNs

In this part, we analyze the effect of number of upper motor neurons, DNs, on maximum total achievable rate across the network so that we can quantify changes on total achievable rates with the upper motor neuron loss. We lack of data regarding average number of functional contacts, T_D, in {DN → MN} links and number of DNs projecting to TA nucleus. Thus, maximum total rate is simulated for different T_D and N_{DN} values. Maximum total rates are obtained with respect to different spiking rates of DN, λ_{DN}'s, with the maximum of 500 Hz.

Fig. 4a shows the maximum total rate of flow of information across the network in the allowable spiking range. As depicted

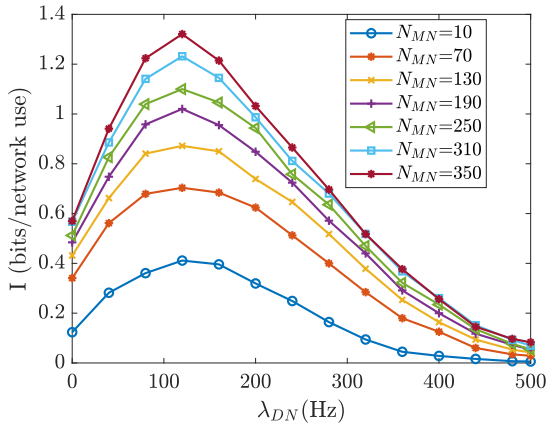

(a) $N_{DN} = 100$, $T_D = 8$

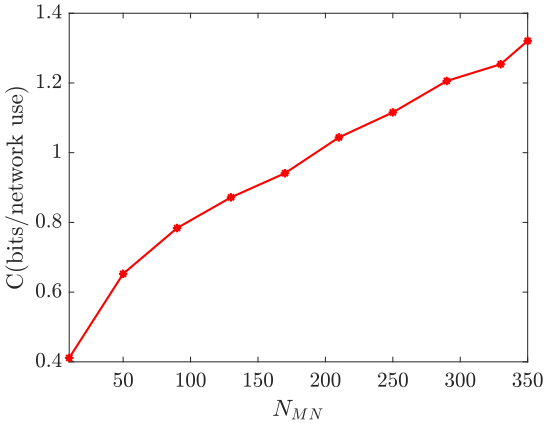

(b) $N_{DN} = 100$, $T_D = 8$

Figure 3: (a) Mutual information and (b) maximum total achievable rates for different number of MNs.

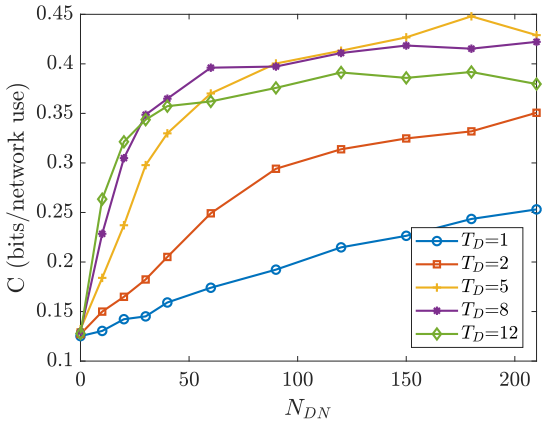

(a) $N_{MN} = 10$

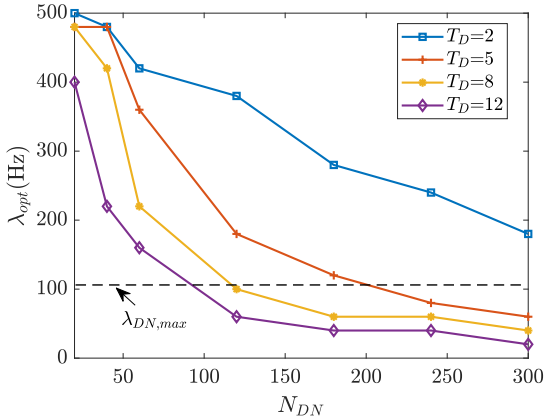

(b) $N_{MN} = 10$

Figure 4: (a) Maximum achievable total rate for different number of functional contacts per DN and (b) optimal spiking rates

in Fig. 4a, maximum total information rate across the network increases with the number of upper motor neurons, N_{DN}, up to a point and then show saturation trend. Moreover, as the number of functional contacts per DN, T_D, increases, maximum total rate that can be attained increases in low N_{DN} range (~ 0 to 40 DNs). This is expected because maximum of the mutual information is not reached in the low N_{DN} range (~ 0 to 40 DNs) in case of low T_D's (1 to 2 T_D's). The result also reveals that in the low T_D range, the network is more prone to capacity decrease when part of upper motor neurons is lost as a result of SCI. Moreover, with relatively lower T_D's, higher maximum total rate can be obtained when high number of DNs such as 200 DNs are recruited in the network. This result is not observable for the cases $T_D = 1, 2$ because higher number of DNs is needed to reach maximum of the mutual information.

Optimal λ_{DN} values achieving maximum total rate are shown in Fig. 4b. When maximum firing rate constraint, i.e., $\lambda_{\text{DN}} \leq \lambda_{\text{DN,max}}$, is applied, maximum total rates are not achievable in low T_D range in any case due to the physical limitations on the firing rate.

4.3 Information Theoretical Metrics and Spinal Cord Dysfunctions

In this part, we deduce the relation between the results obtained via numerical simulations and several reported symptoms of spinal cord dysfunctions. The relation between observed symptoms of several spinal cord diseases and information theoretic metrics, such as maximum total rate and mutual information, can provide an insight regarding communication failures through the spinal cord due to injuries or diseases. Aforementioned metrics may be used in ICT-based diagnosis tools and treatment techniques for SCI.

Loss of lower motor neurons, i.e., MNs, can arise from neurodegeneretive diseases such as amyotrophic lateral sclerosis (ALS) or damage to the cells because of SCI. One of the most profound symptoms of MN loss is weakness in the associated muscle [27]. As illustrated in Fig. 3b, decrease in total maximum rate with decreasing number of MNs is resulting in the weakness in the muscle affected from the injury.

As shown in Fig. 4a, maximum total rate of information flow is not affected significantly from partly loss of DNs up to a critical

number of neuron loss, when DNs have relatively high number of functional contacts. This result is compatible with intrinsic mechanisms of the nervous system evolved to cope with communication failures, in a way that nervous system can compensate the loss of neurons with the exception of cell loss in significant extent by increasing redundancy in the form of functional contact [33] via plasticity. After critical number of cell loss, however, motor actions cannot be performed normally [5].

5 CONCLUSION

In this study, we analyze rate of information flow across a spinal cord motor nucleus system from information theoretical perspective. To this end, we first develop an equivalent single-hop neurospike communication multi-terminal network and then formulate bound on the total achievable rates across the network. Finally, we simulate maximum achievable rates numerically with regard to a particular spinal cord motor nucleus system. The results indicate a correlation between decreasing maximum total rates and weakness in the muscle as a result of lower motor injury.

6 ACKNOWLEDGMENT

This work was supported in part by the ERC projects MINERVA (ERC-2013-CoG #616922) and the ERC Proof of Concept project MINERGRACE (ERC-2017-PoC #780645).

REFERENCES

[1] Naveed A Abbasi and Ozgur B Akan. 2015. A queueing-theoretical delay analysis for intra-body nervous nanonetwork. *Nano Communication Networks* 6, 4 (2015), 166–177.

[2] Ozgur B Akan, Hamideh Ramezani, Tooba Khan, Naveed A Abbasi, and Murat Kuscu. 2017. Fundamentals of molecular information and communication science. *Proc. IEEE* 105, 2 (2017), 306–318.

[3] IF Akyildiz, M Pierobon, S Balasubramaniam, and Y Koucheryavy. 2015. The internet of bio-nano things. *IEEE Communications Magazine* 53, 3 (2015), 32–40.

[4] AbdulRasheed A Alabi and Richard W Tsien. 2012. Synaptic vesicle pools and dynamics. *Cold Spring Harbor perspectives in biology* 4, 8 (2012), a013680.

[5] Francisco J Alvarez, Katie L Bullinger, Haley E Titus, Paul Nardelli, and Timothy C Cope. 2010. Permanent reorganization of Ia afferent synapses on motoneurons after peripheral nerve injuries. *Annals of the New York Academy of Sciences* 1198, 1 (2010), 231–241.

[6] Eren Balevi and Ozgur B Akan. 2013. A physical channel model for nanoscale neuro-spike communications. *IEEE Transactions on Communications* 61, 3 (2013), 1178–1187.

[7] Eren Balevi and Richard D Gitlin. 2018. An Inherent Fog Network: Brain-Spinal Cord-Nerve Networks. *IEEE Access* (2018).

[8] György Buzsáki and Kenji Mizuseki. 2014. The log-dynamic brain: how skewed distributions affect network operations. *Nature Reviews Neuroscience* 15, 4 (2014), 264.

[9] Angela Sara Cacciapuoti, Alessandro Piras, and Marcello Caleffi. 2016. Modeling the dynamic processing of the presynaptic terminals for intrabody nanonetworks. *IEEE Transactions on Communications* 64, 4 (2016), 1636–1645.

[10] Rogerio RL Cisi and Andre F Kohn. 2008. Simulation system of spinal cord motor nuclei and associated nerves and muscles, in a Web-based architecture. *Journal of computational neuroscience* 25, 3 (2008), 520–542.

[11] Thomas M Cover and Joy A Thomas. 2012. *Elements of information theory*. John Wiley & Sons.

[12] Jinfeng Du. 2012. *Cooperative Strategies in Multi-Terminal Wireless Relay Networks*. Ph.D. Dissertation. KTH Royal Institute of Technology.

[13] Leonardo Abdala Elias, Renato Naville Watanabe, and André Fabio Kohn. 2014. Spinal mechanisms may provide a combination of intermittent and continuous control of human posture: predictions from a biologically based neuromusculoskeletal model. *PLoS computational biology* 10, 11 (2014), e1003944.

[14] Andrew Jacob Pixley Fink. 2013. *Exploring a behavioral role for presynaptic inhibition at spinal sensory-motor synapses*. Columbia University.

[15] Alan S Finkel and Stephen J Redman. 1983. The synaptic current evoked in cat spinal motoneurones by impulses in single group 1a axons. *The Journal of Physiology* 342, 1 (1983), 615–632.

[16] Juan A Gallego, Jakob L Dideriksen, Ales Holobar, Jaime Ibáñez, Vojko Glaser, Juan P Romero, Julián Benito-León, José L Pons, Eduardo Rocon, and Dario Farina. 2015. The phase difference between neural drives to antagonist muscles in essential tremor is associated with the relative strength of supraspinal and afferent input. *Journal of Neuroscience* 35, 23 (2015), 8925–8937.

[17] Tooba Khan, Bilgesu A Bilgin, and Ozgur B Akan. 2017. Diffusion-based model for synaptic molecular communication channel. *IEEE transactions on nanobioscience* 16, 4 (2017), 299–308.

[18] M Kuno and JN Weakly. 1972. Quantal components of the inhibitory synaptic potential in spinal motoneurones of the cat. *The Journal of physiology* 224, 2 (1972), 287–303.

[19] Derya Malak and Ozgur B Akan. 2013. A communication theoretical analysis of synaptic multiple-access channel in hippocampal-cortical neurons. *IEEE Transactions on communications* 61, 6 (2013), 2457–2467.

[20] Victor Matveev and Xiao-Jing Wang. 2000. Implications of all-or-none synaptic transmission and short-term depression beyond vesicle depletion: a computational study. *Journal of Neuroscience* 20, 4 (2000), 1575–1588.

[21] Niall J Moore, Gardave S Bhumbra, Joshua D Foster, and Marco Beato. 2015. Synaptic connectivity between Renshaw cells and motoneurons in the recurrent inhibitory circuit of the spinal cord. *Journal of Neuroscience* 35, 40 (2015), 13673–13686.

[22] Neuroelectro.org. 2018. https://https://neuroelectro.org/neuron/177/

[23] Peter C Petersen and Rune W Berg. 2016. Lognormal firing rate distribution reveals prominent fluctuation–driven regime in spinal motor networks. *Elife* 5 (2016).

[24] Joseph P Pierce and Lorne M Mendell. 1993. Quantitative ultrastructure of Ia boutons in the ventral horn: scaling and positional relationships. *Journal of Neuroscience* 13, 11 (1993), 4748–4763.

[25] Arthur Prochazka and Monica Gorassini. 1998. Models of ensemble firing of muscle spindle afferents recorded during normal locomotion in cats. *The Journal of physiology* 507, 1 (1998), 277–291.

[26] Yifat Prut and Steve I Perlmutter. 2003. Firing properties of spinal interneurons during voluntary movement. I. State-dependent regularity of firing. *Journal of Neuroscience* 23, 29 (2003), 9600–9610.

[27] Dale Purves, George J Augustine, David Fitzpatrick, Lawarence C Katz, Anthini-Samuel LaMantia, James O McNamara, and S Mark Williams. 2001. Neuroscience. Sunderland. *MA: Sinauer Associates* (2001).

[28] Hamideh Ramezani and Ozgur B Akan. 2015. Synaptic channel model including effects of spike width variation. In *Proceedings of the Second Annual International Conference on Nanoscale Computing and Communication*. ACM, 11.

[29] Hamideh Ramezani and Ozgur B Akan. 2017. A communication theoretical modeling of axonal propagation in hippocampal pyramidal neurons. *IEEE transactions on nanobioscience* 16, 4 (2017), 248–256.

[30] Hamideh Ramezani and Ozgur B Akan. 2018. Information Capacity of Vesicle Release in Neuro-Spike Communication. *IEEE Communications Letters* 22, 1 (2018), 41–44.

[31] Hamideh Ramezani, Caglar Koca, and Ozgur B Akan. 2017. Rate Region Analysis of Multi-terminal Neuronal Nanoscale Molecular Communication Channel. In *Proceedings of IEEE Nano 2017*. IEEE.

[32] Stephen Redman. 1990. Quantal analysis of synaptic potentials in neurons of the central nervous system. *Physiological Reviews* 70, 1 (1990), 165–198.

[33] Donald G Stein and Stuart W Hoffman. 2003. Concepts of CNS plasticity in the context of brain damage and repair. *The Journal of head trauma rehabilitation* 18, 4 (2003), 317–341.

[34] GJ Stuart and SJ Redman. 1990. Voltage dependence of Ia reciprocal inhibitory currents in cat spinal motoneurones. *The Journal of physiology* 420, 1 (1990), 111–125.

[35] Hakan Tezcan, Sema F Oktug, and Fatma Neşe Kök. 2015. Employing TDMA protocol in neural nanonetworks in case of neuron specific faults. *IEEE transactions on nanobioscience* 14, 6 (2015), 572–580.

[36] Mladen Veletić, Pål Anders Floor, Zdenka Babić, and Ilangko Balasingham. 2016. Peer-to-peer communication in neuronal nano-network. *IEEE Transactions on Communications* 64, 3 (2016), 1153–1166.

[37] Mladen Veletić, Pål Anders Floor, Youssef Chahibi, and Ilangko Balasingham. 2016. On the upper bound of the information capacity in neuronal synapses. *IEEE Transactions on Communications* 64, 12 (2016), 5025–5036.

[38] Anthony Zador. 1998. Impact of synaptic unreliability on the information transmitted by spiking neurons. *Journal of Neurophysiology* 79, 3 (1998), 1219–1229.